Наносистеми, наноматеріали, нанотехнології
Nanosystems, Nanomaterials, Nanotechnologies
2015, т. 13, № 3, сс. 403–414

PACS numbers: 71.20.Tx, 77.84.-s, 81.07.Pr, 81.16.Fg, 82.75.-z, 84.32.Tt, 84.37.+q

Impedance Anisotropy and Quantum Photocapacity of Bio/Inorganic Clathrates InSe<HISTIDINE> and GaSe<HISTIDINE>

F. O. Ivashchyshyn, I. I. Grygorchak, and M. I. Klapchuk

Lviv Polytechnic National University,
12 S. Bandera Str.,
79013 Lviv, Ukraine

Intercalated nanostructures of InSe<htd> and GaSe<htd> are fabricated. Phenomena of the negative photocapacitance and the quantum capacitance are visualized for the first nanostructure. The introduction of histidine between indium selenide layers leads to increasing of conductivity anisotropy ($\sigma_{\parallel}/\sigma_{\perp}$) from 67 to 226. Temperature dependences of a real component of the complex impedance indicate semiconductor mechanism of conductivity along nanolayers with two activation energies of 1.6 meV in low-temperature region and of 0.25 meV in high-temperature one. An appearance of the giant high-frequency negative magnetoresistance and almost 20-fold photosensibility increasing are observed for the second nanostructure. The conductivity anisotropy ($\sigma_{\parallel}/\sigma_{\perp}$) of the nanostructure GaSe<htd> is 10^2. Temperature dependence of a real component of the complex impedance along the layers within the temperature regions $-30°C < t \le 10°C$, $10°C < t \le 30°C$, $30°C < t \le 50°C$ demonstrates cardinally different mechanisms of conductivity. Activation energies are 0.35 in low-temperature interval and 0.69 in high-temperature one. Non-activated conductivity mechanism is observed in the range of temperature $10°C < t \le 30°C$. The parameters of the energy spectrum calculated by means of the Geballe–Pollak theory prior to and after the introduction of histidine into both nanostructures are given. It well correlates with experimental data.

Сформовано інтеркалянтні наноструктури InSe<htd> та GaSe<htd>. Для першої наноструктури візуалізовано ефекти неґативної фотоємности та квантової ємности. Втілення гістидину між шарами селеніду індію приводить до зростання анізотропії електропровідности $\sigma_{\parallel}/\sigma_{\perp}$ від 67 до 226. Температурні залежності реальної складової комплексного імпедансу засвідчують напівпровідниковий механізм провідности вздовж шарів із двома енергіями активації — у 1,6 меВ у низькотемпературній та у 0,25 меВ у високотемпературній областях. Для другої наноструктури

спостерігаються 20-кратне зростання фоточутливости і поява гігантського високочастотного неґативного магнетоопору. Анізотропія електропровідности $\sigma_{\parallel}/\sigma_{\perp}$ наноструктури GaSe<htd> становить 10^2. Температурна залежність реальної складової комплексного імпедансу уздовж шарів у областях температур $-30°C < t \le 10°C$, $10°C < t \le 30°C$, $30°C < t \le 50°C$ демонструє кардинально відмінні механізми електропровідности. Енергії активації становлять 0,35 у низькотемпературному та 0,69 у високотемпературному інтервалах. При температурах $10°C < t \le 30°C$ спостерігається неактиваційний механізм електропровідности. Для двох наноструктур наведено значення параметрів зонного спектру до і після втілення гістидину, обчислені за теорією Джебола–Поллака, які добре корелюють з одержаними експериментальними даними.

Сформированы интеркалянтные наноструктуры InSe<htd> и GaSe<htd>. Для первой наноструктуры визуализированы эффекты отрицательной фотоёмкости и квантовой ёмкости. Внедрение гистидина между слоями селенида индия приводит к росту анизотропии электропроводности $\sigma_{\parallel}/\sigma_{\perp}$ от 67 до 226. Температурные зависимости реальной составляющей комплексного импеданса свидетельствуют о полупроводниковом механизме проводимости вдоль слоёв с двумя энергиями активации — 1,6 мэВ в низкотемпературной и 0,25 мэВ в высокотемпературной областях. Для второй наноструктуры наблюдаются 20-кратный рост фоточувствительности и появление гигантского высокочастотного отрицательного магнетосопротивления. Анизотропия электропроводности $\sigma_{\parallel}/\sigma_{\perp}$ наноструктуры GaSe<htd> составляет 10^2. Температурная зависимость реальной составляющей комплексного импеданса вдоль слоёв в температурных областях $-30°C < t \le 10°C$, $10°C < t \le 30°C$, $30°C < t \le 50°C$ демонстрирует кардинально отличающиеся механизмы электропроводности. Энергии активации составляют 0,35 в низкотемпературном и 0,69 в высокотемпературном интервалах. При температурах $10°C < t \le 30°C$ наблюдается неактивационный механизм электропроводности. Для двух наноструктур приведены значения параметров зонного спектра до и после внедрения гистидина, вычисленные по теории Джеболла–Поллака, которые хорошо коррелируют с полученными экспериментальными данными.

Key words: InSe, GaSe, histidine, clathrates, supramolecular structure, intercalation, impedance spectroscopy, Nyquist diagram, electrical conduction.

Ключові слова: Inse, GaSe, гістидин, клатрати, супрамолекулярна структура, інтеркаляція, імпедансна спектроскопія, Найквістова діяграма, електропровідність.

Ключевые слова: InSe, GaSe, гистидин, супрамолекулярная структура, интеркалирование, импедансная спектроскопия, диаграмма Найквиста, электропроводность.

(Received 28 May, 2015)

1. INTRODUCTION

With rapid development of nanoengineering (nanoelectronics, quantum coherent spintronics, *etc.*) and with related to these sciences necessity to initiate creation of super-high-capacitance accumulators of electric energy, the formation of heterostructured inorganic–inorganic, inorganic–organic, and bio–organic materials attract still more attention of scientists. The ability to realize unique physical and chemical properties [1, 2], sometimes paradoxical, is associated with these materials.

The known methods of obtaining them, such as vacuum deposition, photolithography, synthetic Langmuir–Blodgett techniques, have some limitation caused by limited variability of the choice of different heteroingridients and by problematic synthesis of 'host–guest' configuration, especially synthesis of heteroaggregate ones. By this time, only a small experience gained on this way and made small steps [3, 4]. As far as bionanosemiconductor inorganic multilayered nanohybrids are concerned, nowadays, information on such investigations is lacking at all. Therefore, the aim of this work is to fill, to some extent, the gap in this branch of investigations.

2. RESULTS AND DISCUSSIONS

To form bio-inorganic/semiconductor nanohybrids, in which layered crystals of gallium selenide (GaSe) and indium selenide (InSe) were used as semiconductor matrix, and the aminoacid histidine ($C_6H_9N_3O_2$) was chosen as a biologically active guest element the suggested three-stage scheme of nanoengineering of crystals was used in [5]. The main feature of histidine is that it is a zwitterion (*i.e.*, it possess properties of both anion and cation) with colossal dipole moment.

Formation of the histidine nanolayers in a threefold expanded matrix of indium selenide leads to more than fortyfold increasing of the real component of specific complex impedance and to almost fourfold increasing of the photosensitivity in the direction perpendicular to the plane of nanolayers.

At the same time, the effect of photoinduced 'negative capacitance' is observed: the corresponding low-frequency impedance hodograph branch enters the fourth, inductive quadrant of the complex impedance plane that correlates with the low-frequency oscillation $\mathrm{Re}Z(\omega)$ at illumination (see curve 6 on Fig. 1). In this case, the mechanism of negative photocapacitance is most likely associated with the photoexcitation of electrons from occupied states below the Fermi level and, therefore, with the formation of trap centres for injected electrons with the relaxation time greater than the half-

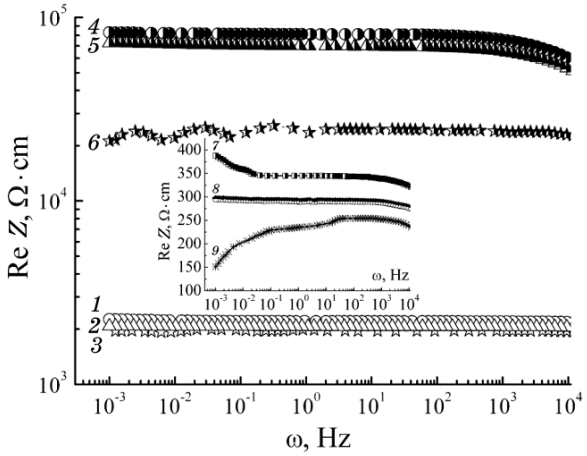

Fig. 1. Frequency dependences of complex impedance perpendicular to the nanolayers of expanded matrix InSe (*1–3*) and of nanostructure InSe<htd> (*4–6*), and along layers InSe<htd> (*7–9*) as measured in the dark (*1*, *4*, *7*) or at illumination (*3*, *6*, *9*), and measured at the action of magnetic field (*2*, *5*, *8*).

period sinusoidal signal.

According to this, the equivalent electric circuit can be represented as shown in Fig. 2. The first parallel high-frequency link $R_1 \| \mathrm{CPE}_1$ (where CPE_1 is element of constant phase capacitive type [6]) in the circuit models the distributed capacitance caused by the presence of vacancies or impurity defects that provide electronic conductivity at room temperature. Second $R_2 \| \mathrm{CPE}_2$, the middle-frequency link, displays the path current flow through energy barriers in guest positions. The low-frequency link $C_Q \| R_{\mathrm{rec}} L$ models the path current flow through the boundary of separation of histidine–semiconductor matrix. Here, R_{rec} is the resistance recombination, which simulates a barrier to charge C_Q, L is the inductance, C_Q is the quantum capacitance [7], which is described by the equation $C_Q = e^2 dn/dE_{Fn}$, where n is the concentration of electrons, E_{Fn} is the energy of the electron Fermi quasi-level. For the last branch of the low-frequency section, admittance can be written as follows:

$$Y(\omega) = \frac{1}{R_{\mathrm{rec}}} - i\omega C \,, \tag{1}$$

where $C = C_L - C_Q$, $C_L = L / R_{\mathrm{rec}}^2$.

According to equation (1), impedance of last link in an equivalent electric circuit for an illuminated nanohybrid at very low frequencies ($\omega < 1/(R_{\mathrm{rec}} C)$) is a parallel connection of recombination resistance and a constant negative capacitance C. Note that, at condi-

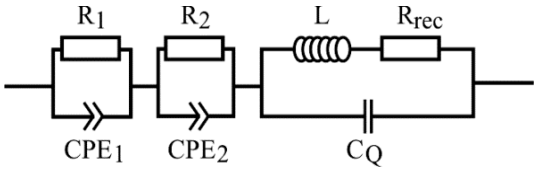

Fig. 2. The equivalent electric circuit.

TABLE 1. The parameters of the band spectrum prior to and after the introduction of histidine into InSe.

	Density of jumping centres near the Fermi level $N(F)\cdot10^{44}$, $J^{-1}\cdot m^{-1}$	Radius of jump $R\cdot10^{-8}$, m	Distribution of trap centres near the Fermi level $J\cdot10^{-23}$, J	Real density of deep trap centres $N_t\cdot10^{22}$, m^{-3}
InSe	32.13	2.90	0.61	1.96
InSe<htd>	2.32	2.39	15.07	3.50

tion C_L C_Q, low-frequency branch comes in IV-inductive quadrant, showing inductive response. Table 1 shows the parameters of the band spectrum prior to and after the introduction of histidine in InSe, which are calculated with the Geballe–Pollak theory. It is evident that histidine encapsulation reduces the density of states at the Fermi level an order of magnitude, which well correlates with low-frequency areas of Re$Z(\omega)$, at the same time, significantly reducing the distribution of trap centres. Radius of jump can be considered stable.

Study of the path current flow along the layers of expanded matrix InSe and nanohybridized structure InSe<htd> in the frequency range of 10^{-3}–1 Hz showed that the conductivity anisotropy ($\sigma_\parallel/\sigma_\perp$) with the introduction of histidine increases from 67 to 226.

The growth of Re$Z(\omega)$ perpendicular to the nanolayers after the introduction of histidine may be caused by decreasing of carrier mobility due to 'rotational' polaron formation, and its falling along them likely caused by the increasing carrier concentration due to the modification of the band structure InSe by the electric field of 'guest' assuming 'ferroelectric' ordering of histidine dipoles along layers as shown in Fig. 3, *a*.

As shown in our work [8] for the latter case along the q-axis of the Brillouin zone, the valence band splits into two subbands; at the same time, widths of subbands reduce comparatively to the unperturbed system.

A similar situation for the conduction band can be obtained. As a result, one of the branches of the valence band arises along the en-

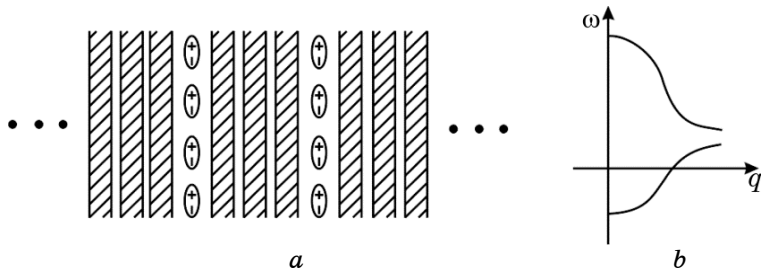

Fig. 3. Ferroelectric arrangement of dipoles (*a*) and the schematic presentation of band structure modification of InSe<htd> layers (*b*).

ergy scale 'up' and one of the branches of the conduction band goes 'down' (Fig. 3, *b*). As a consequence, the effective bandgap decreases or conduction band catch the Fermi level; this leads to increasing of the concentration of carriers.

Photosensitivity along layers of InSe<htd> is almost twice less than perpendicular to them, while for the expanded matrix, these values are virtually identical. When they are illuminated, it is observed anomalous frequency dependence Re$Z(\omega)$; it is the monotonic growth with increasing frequency in fairly wide frequency range (curve *9* in Fig. 1). In this case, low-frequency branch of the hodograph of the impedance is almost parallel to ReZ-axis with opposite its genesis ω as well as to the relevant branch of hodograph built to measure in the dark. If the latter are modelled by finite element of constant phase (BCPE) [6], which reflects the path current flow in space-restricted area with the complex electrical conductivity, then at illumination, one can proposed a model of impedance along the layers containing the link with quantum capacity Lurie [7]. In this case, it represents a contribution from the histidine nanoclusters with the energy spectrum of the path current flow caused by the nonequilibrium carriers. As a result, a conductivity of nonequilibrium carriers due to gravity in accordance with the [9] should decrease with increasing frequency, as observed in Fig. 1 (curve *3*).

Temperature dependences of the real component of the complex impedance along the layers (Fig. 4) indicate semiconductor nature of the electrical conductivity of nanohybrids with two activation energies: 1.6 meV in low-temperature region and 0.25 meV in high-temperature one. It is interesting to note that for proper temperature of change of conductivity mechanism at (–10°C) corresponds to a radical change of the low-frequency branch of Nyquist diagrams: the passing to the fourth, inductive, quadrant (inset to Fig. 4). This makes it possible to assume that, at temperatures higher than –10°C, electrons captured by trap centres would be delocalized. With reducing the temperature to –30°C, localized electrons no

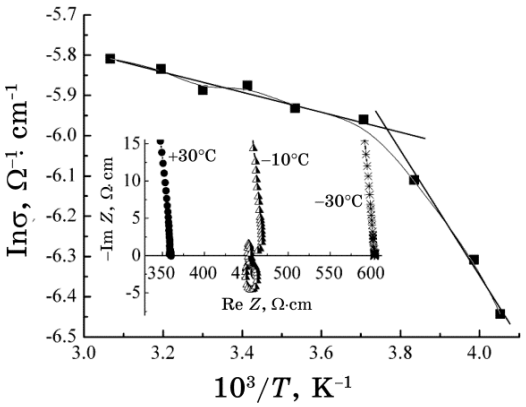

Fig. 4. Temperature dependences of a real component of impedance along nanolayers InSe<htd>. In the inset to Fig. 4, hodograph of impedance is given.

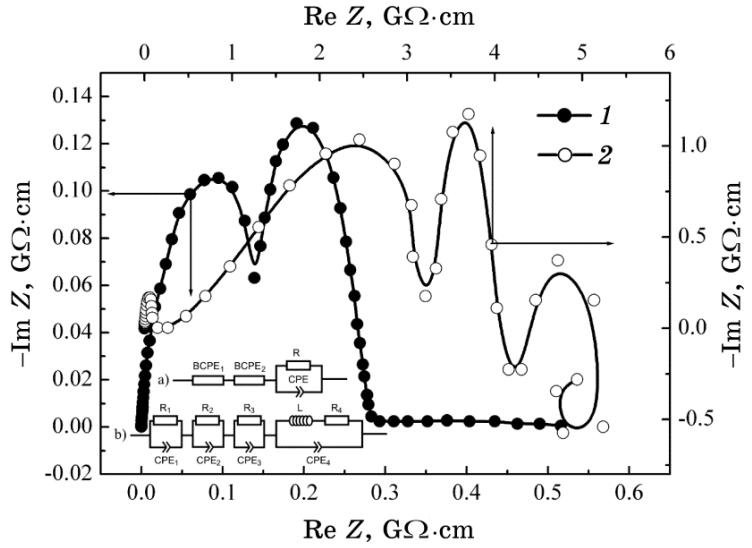

Fig. 5. Nyquist diagram measured in the dark for the initial expanded matrix GaSe (*1*) and for the nanostructure GaSe<htd> (*2*) (with equivalent electric circuits corresponding to them).

longer is delocalized in the tails of the density of states.

For the initial expanded matrix (curve *1* in Fig. 5), we have usual situation: the corresponding hodograph of impedance is of two-arc form, and it represents capacitive response of localized states and the frequency depended impedance proper caused by jumps between localized states near the Fermi level in the packet of atomic mono-

layers (high-frequency curve). The middle-frequency curve represents the path current flow through widened spaces of actions of the van der Waals forces. These arcs are modelled by means of bounded element of constant phase (BCPE), which represents the path of current flow in space-restricted domain of complex-valued electric conductance [10]. The low-frequency section represents the distribution of active resistance element (caused by discretization of the energy spectrum of the expanded matrix of gallium selenide), this resistance is modelled by means of constant phase element CPE with low value of phase deviation $\zeta < 0.1$ [6].

The equivalent electric circuit in this case is given in the inset (a) to Fig. 5. The introduction of histidine leads to the increase in frequency dispersion of the hodograph of the impedance, and it indicates the emergence of additional potential barriers. Accordingly, the equivalent electric circuit is as shown in inset (b) in Fig. 5. The last link contains induction (inset (b) in Fig. 5) because the low-

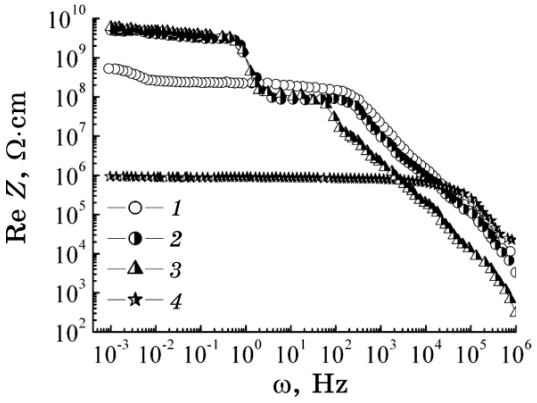

Fig. 6. Frequency dependences of a real component of impedance perpendicular to the layers for initial expanded matrix GaSe measured in the dark (*1*) and for nanostructure GaSe<htd> measured in the dark (*2*) as well as at illumination (*4*), and measured at the action of magnetic field (*3*).

TABLE 2. The parameters of the energy spectrum prior to and after the introduction of histidine in GaSe.

	Density of jumping centres near the Fermi level $N(F)\cdot10^{43}$, $J^{-1}\cdot m^{-1}$	Radius of jump $R\cdot10^{-8}$, m	Distribution of trap centres near the Fermi level $J\cdot10^{-22}$, J	Real density of deep trap centres $N_t\cdot10^{22}$, m^{-3}
GaSe	6.56	3.02	2.63	1.73
GaSe<htd>	10.60	2.83	1.99	2.10

frequency branch of the Nyquist diagram passes to the induction quadrant IV of the plane of complex-valued impedance. This indicates the phenomenon of 'negative capacitance'.

The introduction of histidine between selenide layers leads to twenty-fold growth of the real component of complex impedance in the low-frequency spectrum (10^{-3}–1 Hz) (Fig. 6). Lighting of the nanostructures GaSe<htd> causes a decrease of Re$Z(\omega)$ almost by $5 \cdot 10^3$ times in the specified frequency range (curve *4* in Fig. 6). The latter phenomenon is quite expected, as semiconductor matrix is photosensitive in the visible spectrum. However, compared to the enhanced matrix implementation <htd> leads to an almost 20-fold increasing of photosensitivity. At the same time, Figure 6 (curve *4*) shows the previously non-observed effect of the giant high-frequency negative magnetoresistance: in the frequency range $60 < \omega \le 10^6$ Hz, magnetic field strength of 2.75 kOe at room temperature leads to a more than 5-fold reduction of Re$Z(\omega)$. Taking into account no practical visualization of the magnetoresistance at lower frequencies, this effect can most likely be associated with Zeeman delocalization of charge carriers from the deeper trap centres. Table 2 shows the parameters of the energy spectrum before and after the introduction of histidine in GaSe as calculated within the Geballe–Pollak theory. In contrast to InSe, one can see a decrease of density of jumping centres and distribution of trap levels near the Fermi level.

Behaviour of hodograph of impedance along the impedance layers GaSe<htd> has the same character as in the measurement perpendicular, with the exception of the magnetic field. In this case, the frequency dispersion growth and middle/high-frequency branches of

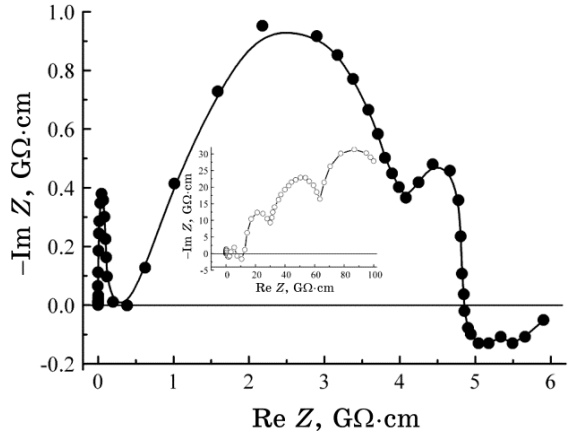

Fig. 7. Nyquist diagram GaSe<htd> perpendicular to the layers and along them (see inset).

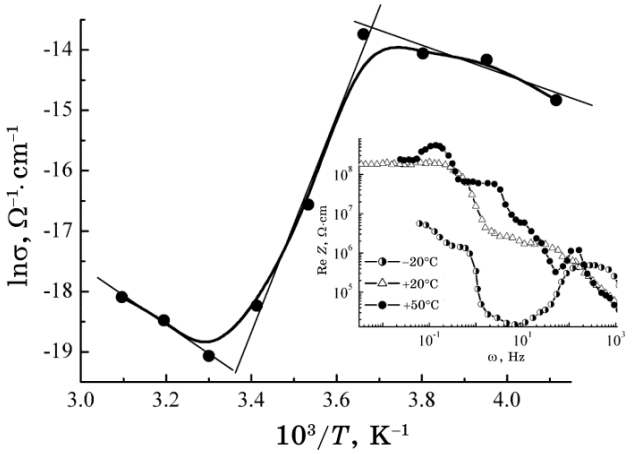

Fig. 8. Temperature dependences of a real component of impedance along nanolayers GaSe<htd>. In the inset, their frequency dependences are given.

Nyquist diagrams 'pass' in inductive quadrant of the plane of complex-valued impedance (see the inset in Fig. 7). This is to some extent correlated with the above discussed Zeeman localization (delocalization) of charge carriers.

Investigation of the path current flow along the layers of nanohybridized structure GaSe<htd> showed that, in the frequency range (10^{-3}–1 Hz), electrical conductivity anisotropy is $\sigma_{\parallel}/\sigma_{\perp} \approx 10^2$, and reduction of the real component of the complex impedance at illumination reaches tenfold value. In contrast to the previous measurement geometry, in this case, positive magnetoresistance is visualized at lower frequencies from 10^{-2} Hz: Re$Z(\omega)$ in a magnetic field is growing more than twice. In this case, high-frequency negative magnetoresistance not only preserved in the same frequency range, but its increasing reaches almost 14-fold value. Obviously, this is an indication of different energy structure in perpendicular and along the layers direction.

The temperature dependence for GaSe<htd> along the layers demonstrates cardinally different mechanisms of conductivity at temperature regions $-30°C < t \le 10°C$, $10°C < t \le 30°C$, $30°C < t \le 50°C$ (Fig. 8). If the first and last temperature ranges correspond to the activation mechanism, then one can obtains non-activation mechanism of conductivity in the range of temperatures $10°C < t \le 30°C$.

3. CONCLUSIONS

The introduction of histidine into three-fold expanded matrix of indium selenide leads to forty-fold increasing of a real component

of specific complex impedance and almost four-fold increasing of photosensibility in direction perpendicular to nanolayers.

An appearance of photoinductive 'negative photocapacitance' is observed for nanostructure InSe<htd>; the mechanism of this phenomenon is most likely associated with the photoexcitation of electrons from occupied states below the Fermi level and, therefore, with the formation of trap centres for injected electrons with the relaxation time greater than the half-period sinusoidal signal.

The conductivity anisotropy ($\sigma_{\parallel}/\sigma_{\perp}$) due to the introduction of histidine into extended matrix of InSe<htd> increases from 67 to 226 in the frequency range of 10^{-3}–1 Hz.

Temperature dependence of a conductivity of the InSe<htd> nanostructure has a semiconductor character with two activation energies of 1.6 meV and 0.25 meV.

The introduction of histidine into three-fold expanded matrix of gallium selenide leads to twenty-fold increasing of a real component of specific complex impedance and twenty-fold increasing of photosensibility in direction perpendicular to nanolayers.

The evidence of a giant high-frequency negative magnetoresistance is observed for nanostructure GaSe<htd> in constant magnetic field with strength of 2.75 kOe at room temperature; magnetic field leads to a more than 5-fold reduction of $\mathrm{Re}Z(\omega)$ in the frequency range $60 < \omega \leq 10^6$ Hz.

The conductivity anisotropy ($\sigma_{\parallel}/\sigma_{\perp}$) for the GaSe<htd> nanostructure is 10^2, and decrease of a real component of the complex impedance at illumination reaches ten-fold value. At the same time, positive magnetoresistance is visualized at frequencies less than 10^{-2} Hz: there is $\mathrm{Re}Z(\omega)$ growth by more than twice in magnetic field, and high-frequency negative magnetoresistance growth is reaching almost 14-fold value.

REFERENCES

1. J. H. Choy, S. J. Kwon, and G. S. Park, *Science*, **280**: 1589 (1998).
2. J. H. Choy, S. Y. Kwak, J. S. Park, Y. J. Jeong et al., *J. Am. Chem. Soc.*, **121**: 1399 (1999).
3. I. Grygorchak, F. Ivashchyshyn, P. Stakhira et al., *Journal of Nanoelectronics and Optoelectronics*, **8**, No. 3: 292 (2013).
4. T. M. Bishchaniuk and I. I. Grygorchak, *Applied Physics Letters*, **104**: 203104-1 (2014).
5. F. Ivashchyshyn, I. Grygorchak, P. Stakhira et al., *Journal of Experimental Nanoscience*, **9**, No. 7: 678 (2014).
6. Z. B. Stojnov et al., *Electrochemical Impedance* (Moscow: Nauka: 1991) (in Russian).
7. S. Luryi, *Appl. Phys. Lett*, **52**, No. 6: 501 (1988).
8. F. Ivashchyshyn I. Grygorchak, O. Sudakova et al., *Materials Science &*

Technology, **27**, No. 11: 973 (2011).
9. V. L. Bonch-Bruevich and S. G. Kalashnikov, *Semiconductor Physics* (Moscow: Nauka: 1977) (in Russian).
10. *Impedance Spectroscopy. Theory, Experiment, and Applications. 2nd Edition* (Eds. E. Barsoukov and J. R. Macdonald) (Hoboken, NJ: John Wiley & Sons: 2005).